ARMA 15-0175

Relative Importance of THM Effects during Non-isothermal Fluid Injection in Fractured Media

Jalali, M.R. and Evans, K.F.
ETH Zurich, Department of Earth Sciences, Zurich, Switzerland
Valley, B.C.
University of Neuchâtel, Centre for Hydrogeology and Geothermics (CHYN), Neuchâtel, Switzerland
Dusseault, M.B.
University of Waterloo, Department of Earth and Environmental Sciences, Waterloo, Ontario, Canada

This paper was prepared for presentation at the 49th US Rock Mechanics / Geomechanics Symposium held in San Francisco, CA, USA, 28 June- 1 July 2015.

ABSTRACT: Rock mass treatment using fluid injection is common in various industrial applications, including enhanced recovery methods in the oil and gas industry, rock mass pre-conditioning in the mining industry, and heat extraction in geothermal systems. Non-isothermal fluid injection requires consideration of the thermomechanical perturbation as well as hydro-mechanical processes. Thermal effect is rarely included in injection analysis for geothermal application and thermal enhanced oil recovery methods, although with long times their impact becomes of first-order. In this paper, a fully-coupled, hybrid numerical model is implemented to study the effect of cold fluid injection into a conductive fracture under different injection/cooling schemes. The results show that the thermoelastic effect soon overwhelms the hydroelastic effect adjacent to the injection source, whereas far from the injection point, hydroelastic effect dominates because the pressure front always moves faster than the cold front. In addition, the fracture becomes more susceptible to shear failure in the presence of both thermoelastic and hydroelastic induced stresses for the case of cold fluid injection. The magnitude of the changes implies that an appropriate thermo-hydromechanical (THM) model is an essential key to address the physical behavior and potential impairment of fracture conductivity under thermal stimulation.

1. INTRODUCTION

Rock mass treatment using fluid injection is common in various industrial applications. Fluid is usually injected under a constant rate or injection pressure to fulfill the intended engineering goal of the stimulation practice. In the oil and gas industry, as an example, large volumes of water are injected at constant pressure during secondary recovery phase for waterflooding the oil-bearing reservoirs with low pressure (with respect to the minimum principal stress) to displace part of the remaining oil toward the production well [1]. In the mining industry, rock mass pre-conditioning using hydraulic fracturing may soon become standard practice for stope mining to facilitate caving propagation and fragmentation management [2]. On-going research interests are pursuing fluid injection as an in-situ stress and rock mass stiffness management tool [2, 3].

Hydraulic stimulation for enhanced geothermal systems (EGS) is associated with creation of new fractures or dilation of existing fractures around the injection and production boreholes in order to reduce the wellbore effect and increase the rock mass injectivity and thermal productivity. If the initial injection pressure exceeds the minimum stress, $p_{inj} > \sigma_3$, hydraulic fractures are created either by opening pre-existing weakness planes, or, less commonly, generating new fractures through intact rock. Also, cold fluid injection at a pressure below the fracture pressure can lead to loss of compressive stress through thermoelastic shrinkage. Induced shear dilation with attendant permanent fracture opening within the stimulated volume is a goal for the design and creation of heat exchangers in EGS reservoirs [4].

The complexity inherent in these examples is large because of induced temperature changes; i.e., non-isothermal fluid injection affects the physical behavior of the host rock through volume changes and concomitant stress redistribution. In this case additional thermomechanical components must be added to the existing hydromechanical processes as well as dependency of viscosity and density to temperature variation. These additional effects are significant,

particularly for geothermal applications and thermal enhanced oil recovery methods.

The presence of natural fractures and discontinuities in the host rock increases the heterogeneity of the system and adds a strong non-linearity to the transport processes. In such a situation, it is unclear *a priori* if the thermomechanical response is significant or not, compared with the hydromechanical response, over the time-scale of the process. An appropriate understanding of Δp- and ΔT-induced stress effects on the dominant conductive fracture network then becomes crucial to understand and predict the physical behavior of the system.

This paper assesses the conditions under which the thermomechanical rock response component cannot be neglected, by examining induced thermoelastic and poroelastic stress effects on the elastic deformation and failure behavior of a conductive fracture in an isotropic and homogenous impermeable medium. The governing equations of a THM-coupled system are presented and defined. A fully coupled thermo-hydromechanical hybrid model is developed via a combination of the finite difference method and the displacement discontinuity method (FDM-DDM). This model is then used to simulate the physical behavior of a single conductive fracture under different injection/cooling scenarios. A sensitivity analysis is performed to study the elastic deformation and failure behavior of the conductive fracture during fluid injection/cooling. In this analysis the effect of fracture orientation in a differential stress field, injection flow rate and injection temperature on the failure potential of the conductive fracture is considered.

2. THERMO-HYDROMECHANICAL (THM) GOVERNING EQUATIONS

Thermo-poroelasticity describes the coupling of pore pressure, temperature, stress and deformation in a deformable, fluid-saturated porous medium by combining the linear momentum conservation equation with Hooke's law, the fluid mass conservation equation with Darcy's law, and the energy conservation equation with Fourier's law. These three governing equations for single-phase Newtonian fluid flow in an isotropic, homogenous and linearly elastic porous medium may be written as [5]

$$G u_{i,jj} + (\lambda + G) u_{j,ji} - \alpha p_{,i} - \beta_s K_b T_{,i} = 0 \qquad (1)$$

$$\alpha \varepsilon_{vol,t} + \frac{1}{M} p_{,t} + \varphi_0 (\beta_f - \beta_s) T_{,t} = \boldsymbol{\kappa}_p p_{,ii} \pm q_s^f \qquad (2)$$

$$\rho_b C_b \frac{\partial T}{\partial t} + \rho_f C_f \mathbf{q}^f \nabla T = \nabla . (\mathbf{k}_T \nabla T) \pm q_s^h \qquad (3)$$

Here, G is shear modulus, λ is Lamé's first parameter (drained conditions), α and M are Biot's effective stress coefficient and Biot's modulus, respectively, K_b is bulk modulus (drained conditions), ε_{vol} is volumetric strain, φ_0 is initial porosity, β_s and β_f are respectively the solid and fluid thermal expansion coefficients, $\boldsymbol{\kappa}_p$ (= k_{ij}/μ) is the fluid mobility tensor, k and μ are intrinsic permeability and fluid dynamic viscosity, ρ_b (= $\varphi_0\rho_f$ + $(1-\varphi_0)\rho_s$), ρ_f, and ρ_s are the densities of the bulk material, the fluid, and the solid constituent, respectively, C_s and C_f are solid and fluid specific heat capacities at constant fluid pressure, $\mathbf{k}_T$ is bulk thermal conductivity, $\mathbf{q}^f$ is the Darcy velocity of the fluid, and q_s^f and q_s^h are the fluid and heat source and sink terms, respectively. The unknown parameters in these three equations are the displacement vector (**u**), the fluid pressure (p) and the rock or fluid temperature (T).

It should be noted that the Einstein convention is adopted for the indices in the formulations. Also, the classical continuum mechanics sign convention is considered for displacement and stress, i.e. elongation or tension is positive whereas contraction or compression is negative. However, pore pressure compression is considered as positive. Eqs. (1) and (2) are fully coupled via sharing pressure and volumetric strain changes. The effect of volumetric strain (mechanical effect) on temperature variation in Eq. (3) is taken to be negligible. However, the effect of temperature on deformation changes is explicitly considered (Eq. (1)). Solving these governing equations simultaneously provides a fully-coupled deformation, pressure and temperature response of the porous medium to the applied boundary conditions. Eqs. (1) to (3) are the basis of the thermo-poroelastic displacement discontinuity method which is implemented in this paper to study the thermoelastic and poroelastic response of elastic deformable fractures.

3. FULLY COUPLED FDM-DDM MODEL

Various hybrid numerical methods have been used to simulate the THM behavior of fractures. These methods combine different numerical methods so as to reap the benefits from each of the combined methods while optimizing computational time. Although there are no commercial fully-coupled THM hybrid models that can consider all the physical mechanisms involved with fractured media behavior, it is possible to select a specific hybrid model based on the objective of the simulation.

The finite difference - displacement discontinuty method - FDM-DDM - is a suitable hybrid numerical approach for the simulation of elastic and failure THM behavior of conductive fractures in an isotropic and homogenous elastic medium [6]. FDM is implemented to simulate

fluid flow and heat transfer in the fractures. The resultant fluid pressure and temperature distribution are applied as the inner boundary condition for the DDM computations to estimate displacement, stress, temperature and pressure (in the case of a permeable medium) in the surrounding host rock. Cubic law is used to relate the hydraulic aperture variation to the fracture conductivity changes assuming a laminar flow between two parallel plates [7, 8]. The concept of this hybrid method is summarized in Fig. 1.

A hyperbolic law is used to describe the fracture normal stiffness as a function of effective normal stress across the fracture plane [9, 10] as

$$K_n = \frac{\partial \sigma'_n}{\partial D_n} = \frac{K_{ni}}{\left[1 - \sigma'_n / (K_{ni} D_{n\,max} + \sigma'_n)\right]^2} \qquad (4)$$

Here, K_n is the fracture normal stiffness, σ'_n is the effective normal stress, K_{ni} is the fracture normal stiffness at zero effective normal stress, D_n is the fracture closure and $D_{n\,max}$ is the maximum fracture closure.

Fracture shear stiffness is taken as a constant up to the peak shear stress. The peak shear stress is estimated using a Mohr-Coulomb (M-C) criterion and pre-shear elastic behavior. Beyond the peak shear stress, the fracture shear stiffness taken a zero (sliding fracture). Dilation angle is taken as a constant that is dependent upon effective normal stress level during sliding, and is otherwise zero. A summary of different fracture states with their specifications and assumptions in the FDM-DDM model is given in Table 1. More information on the formulation and implementation of FDM-DDM model can be found in [6].

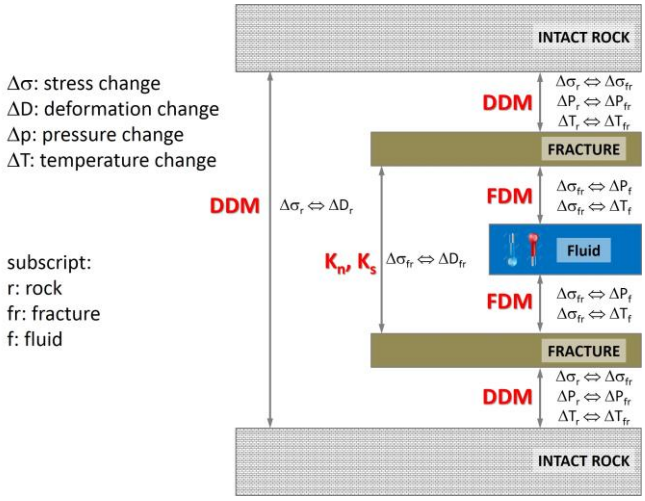

Fig. 1. Fluid-rock interaction in a fractured medium subjected to ΔT and Δp using FDM-DDM.

4. THM BEHAVIOR OF A CONDUCTIVE AND ELASTIC FRACTURE UNDER DIFFERENT INJECTION/COOLING SCENARIOS

In this example, a viscous fluid (i.e. water) is injected into a 100 m long vertical fracture with a constant rate of 3×10^{-9} m^3/s/m and temperature of 30°C for 20 hours. The fracture is symmetrical about the injection borehole, and penetrates rock that has an initial temperature of 80°C (i.e. ΔT = -50°C). The rock is taken as impermeable, and supports a maximum horizontal stress (σ_{yy}) of 35 MPa and a minimum horizontal stress (σ_{xx}) of 20 MPa. In this case, it is reasonable to model the problem with a plane-strain assumption in a horizontal cross-section plane perpendicular to the injection well axis (Fig 2). The fracture azimuth strikes at 60° to the *x*-axis. Thermal, hydraulic and mechanical properties of the fracture and host rock are presented in Table 2.

Table 1. Different fracture states with their specifications and assumptions. Note that the continuum mechanics convention of stress positive in tension but pore pressure positive in compression is used.

Fracture Status	Contact Porosity*	Stress Condition	Fracture Pressure	Fracture Properties
closed fracture	$n_c = 0$	$\sigma_n' < 0$	$p = 0$	$K_n \to \infty$, $\psi = 0$
compliant fracture	$0 < n_c < 1$	$\sigma_n' < 0$ $\lvert\sigma_s\rvert < c + \lvert\sigma_n'\rvert \tan\phi$	$0 < p < \sigma_n$	$K_n = \partial\sigma_n/\partial u_n^{**}$, $\psi = 0$
Mohr – Coulomb Criteria ($\lvert\sigma_s\rvert = c + \lvert\sigma_n'\rvert \tan\phi$)				
sliding fracture	$0 < n_c < 1$	$\sigma_n' < 0$ $\lvert\sigma_s\rvert > c + \lvert\sigma_n'\rvert \tan\phi$	$0 < p < \sigma_n$	$K_n = \partial\sigma_n/\partial u_n^{**}$ $K_s = 0$, $\psi \neq 0$
open fracture	$n_c = 1$	$\sigma_n' \geq 0$	$p \geq \sigma_n$	$K_n = \partial\sigma_n/\partial u_n^{**}$, $\psi = 0$

*Contact porosity is defined as the ratio of non-contacting fracture area to nominal area.
**Fracture normal stiffness is updated based on the hyperbolic model.

In order to better understand the elastic response of a conductive fracture to ΔT and Δp, three different scenarios are considered:

- *Hydro-mechanical case (HM)* where an isothermal fluid (ΔT = 0) is injected in the middle of a fracture at a constant flow rate.
- *Thermo-mechanical case (TM)* in which a constant cold source is applied as a line source in the middle of the fracture (point source for 2-D plane strain) (Δp = 0).
- *Thermo-hydro-mechanical case (THM)* in which hydro-mechanical effects on the fracture elastic behavior are coupled with thermoelastic stress changes, i.e., both ΔT and Δp.

In all simulations, the effect of temperature on viscosity and fluid density is not considered.

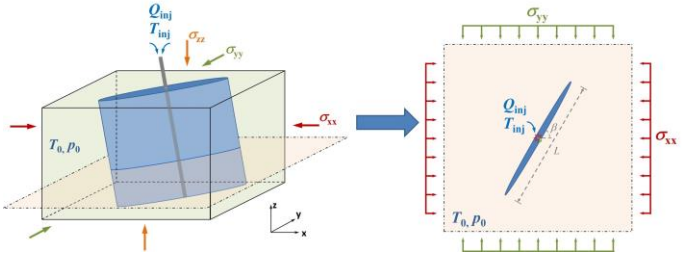

Fig 2. Schematic representation of the single vertical fracture in 3-D (left) and its horizontal cross-section (right). The 3-D problem can be simplified to a 2-D plane-strain problem.

Table 2. Thermal, hydraulic and mechanical properties of the single fracture and adjacent rock.

Mechanical Properties	
Young's modulus (E)	20 GPa
Poisson's ratio (ν)	0.25
Minimum horizontal stress (σ_{xx})	20 MPa
Maximum horizontal stress (σ_{yy})	35 MPa
Fracture normal stiffness at zero effective normal stress (K_n)	10^3 GPa/m
Fracture shear stiffness (K_s)	100 GPa/m
Cohesion (c)	0
Friction angle (ϕ)	30
Dilation angle (ψ)	0
Hydraulic Properties	
Initial fluid pressure (p_0)	10 MPa
Fracture hydraulic aperture at zero effective normal stress (w_0)	10 μm
Residual fracture aperture (w_{res})	1 μm
Fluid compressibility (c_f)	7×10^{-10} 1/Pa
Fluid dynamic viscosity (μ)	10^{-9} MPa.s
Fluid density (ρ_f)	1000 kg/m^3
Contact porosity (n_c)	0.8
Injection fluid rate (Q_{inj})	3×10^{-9} m^3/s/m
Thermal Properties	
Initial temperature (T_0)	80°C
Fluid thermal conductivity (k_T)	0.6 J/m°Ks
Fluid specific heat (C_f)	4200 J/kg°K
Rock heat diffusivity (c^T)	1.6×10^{-6} m^2/s
Fluid thermal expansion (β_f)	2.4×10^{-5} 1/°K
Rock thermal expansion (β_s)	2.1×10^{-5} 1/°K
Injection temperature (T_{inj})	30°C

The pressure and temperature profiles along the fracture after 10 and 20 hours injection for the three scenarios are shown in Fig 3. Since the fracture is embedded in an impermeable medium, injection results in progressive pressurization with a superposed gradient reflecting flow resistance. The pressure profiles at both times for the HM case are everywhere slightly greater than the THM profiles. This is because cooling down the fracture walls in the THM model reduces the effective normal stress resulting in additional driving force for fracture elastic opening, greater fracture volume and thus lower pressure. The pressure gradients in both cases drop slightly over time as the fracture become wider and the permeability increases. Cooling the fracture only at the borehole without any fluid flow (TM case, $\Delta p = 0$) leads to a negligible drop in the fracture pressure profile from its initial 10 MPa value, again as a result of fracture volume increase due to rock cooling.

Temperature propagates with two heat transfer mechanisms, advection and conduction. Heat conduction occurs in both the fracture and rock whereas heat advection dominates in the fracture in the presence of Δp-driven propagation. No heat transfer occurs in the isothermal HM case, whereas only heat conduction occurs in the TM case from a point source (plane strain assumption). For the THM case, heat transfer in the system occurs through a combination of heat advection in the fracture and conduction in the rock. Note that temperature dependency of fluid density and viscosity are not included in this modeling and a change of fluid temperature only (TM case) is assumed to not induce fluid flow (convection cells). If advective flux is reasonable and ΔT moderate for water flow, these simplifications are acceptable for a first-order comparison of mechanisms. Comparing the temperature profile between TM and THM cases shows that heat advection impacts a much larger area than only heat conduction, as the thermal front moves proportional to the fluid front.

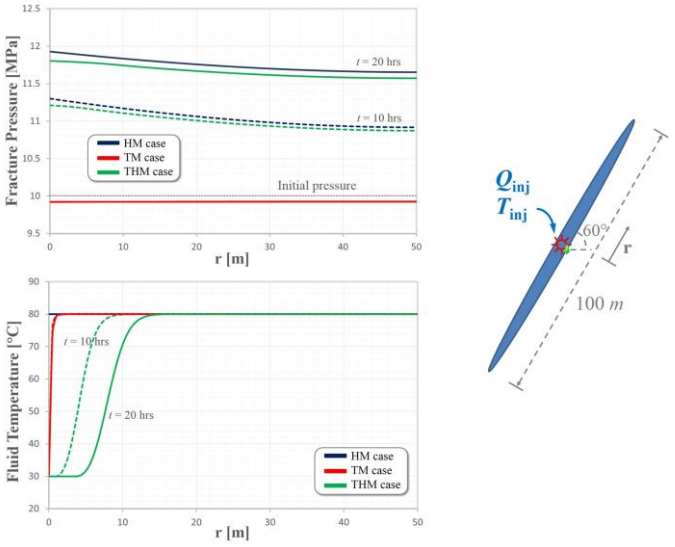

Fig 3. Fracture pressure and temperature along the half length of the studied vertical fracture for three scenarios, i.e. HM, TM, and THM cases after 10 and 20 hours injection.

ΔT and Δp cause total and effective stress changes on the fracture plane as well as its surrounding medium. In order to study the stress changes that had occurred for each of the scenarios after 20 hours, and determine the fracture state at that time (i.e. to see if failure had occurred), the Mohr circles are constructed. These are shown in Fig 4. Note that total stresses are used in order to differentiate between ΔT and Δp effects. Fracture fluid pressure changes do not have any effect on the total stress as the host rock is deemed impermeable (shale or granite) at the time scale of the model and the induced poroelastic stress on the matrix is therefore zero. The

effects of fracture pressure changes are presented by moving the M-C failure line (MCFL) toward the right which is equivalent to shifting the Mohr circle toward left by the pore pressure in an effective stress plot. As mentioned earlier, the amount of pressure increment is not identical between HM and THM cases.

Stress changes induced by thermomechanical effects shift the Mohr circle to the left because cooling results in total stress reduction, however the amount of reduction is different for the TM and THM cases. Although the temperature boundary condition for both TM and THM cases are identical, the cooling front is radially symmetric in TM case, which is a geometry that gives rise to large changes in normal stress, albeit highly localized.

Based on the Fig 4, it is clear that cooling of the rock for 20 hours in cases TM and THM leads to the failure criteria being met or exceeded at the borehole. Fig 5 shows the length of failure (summing both sides of the fracture) as a function of time for the three cases. Failure occurs whenever shear stress, σ_s, satisfies $|\sigma_s| \geq |(\sigma_n - p)\tan\phi|$ where ϕ is the friction angle. The steps for the THM case denote the time increments.

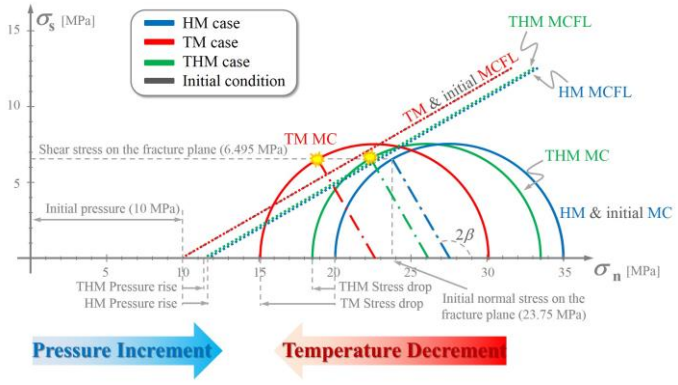

Fig 4. Mohr circle presentation of the stress state prevailing at the borehole for the three different scenarios after 20 hrs of injection and/or cooling. The geomechanics convention of compression positive is used for this figure. The solid line in Mohr semi-circle for total stress, and the dotted line is the Mohr-Coulomb failure line for a friction angle of 30°. The dash-dotted line represents the total normal and shear stresses on the fracture plane.

The failure length for the HM case is zero during the entire injection period. For the TM case, failure is restricted to the vicinity of the cooled borehole where only one element along the fracture fails. Discretization steps along the fracture are 50 cm long and so is the estimated failure length. This means that the thermal perturbation and associated stress changes did not propagate for more than 50 cm during the 20 hours, as is evident in the temperature profile along the fracture shown in the lower-right inset to Fig 5. The short penetration distance is because heat transfer occurs solely by thermal conduction for this case. For the THM case, the failure length progressively increases over time to attain a maximum value of 11.5 meters after 20 hours (the steps in Fig 5 reflect the time increments and the discretization interval). Snapshots of the temperature profile prevailing along the fracture at selected times are shown as the insets in this figure. A measurement of the extent of cooling penetration is given by the 'cooled length', which denotes the fracture length where temperature $T \leq 55$°C, the arithmetic mean of the initial and injected temperature.

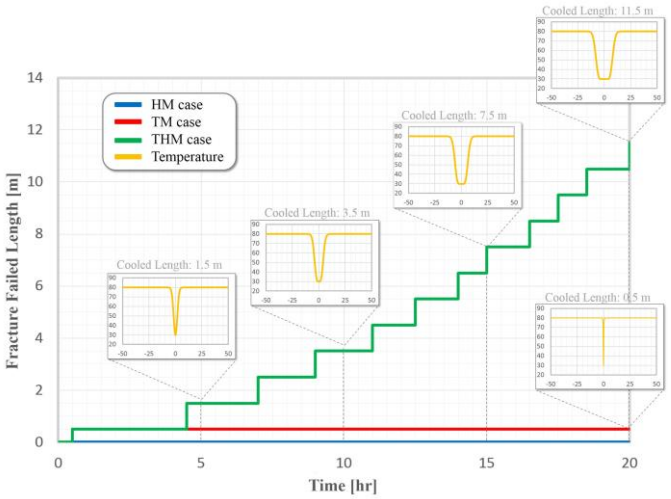

Fig 5. Evolution of the failed length of the fracture (includes both sides) based on the M-C criterion over 20 hours of fluid injection and/or cooling for the three cases. The profiles of temperature along the fracture for several times are shown by the insets. A reasonable correlation between cooled length and fracture failed length is achieved.

The profiles of total and effective normal stresses together with temperature along the fracture after 20 hours (the end of injection/cooling) are shown in Fig 6. For the THM case, both the increased pressure and decreased temperature cause a reduction in effective normal stress in the vicinity of the borehole. However, the similarity of the effective and total stress profiles near the borehole indicates that the effect of temperature is more significant than the pressure effect in this example (a more rapid injection rate would diminish the effect of temperature). A zone of enhanced compressive normal stress occurs immediately beyond the cooling-induced reduced normal stress zone for both TM and THM cases, which is of course the result of stress equilibrium along the fracture plane. In other words, stresses cannot be lost or created, only redistributed, as long as the boundary loads remain constant.

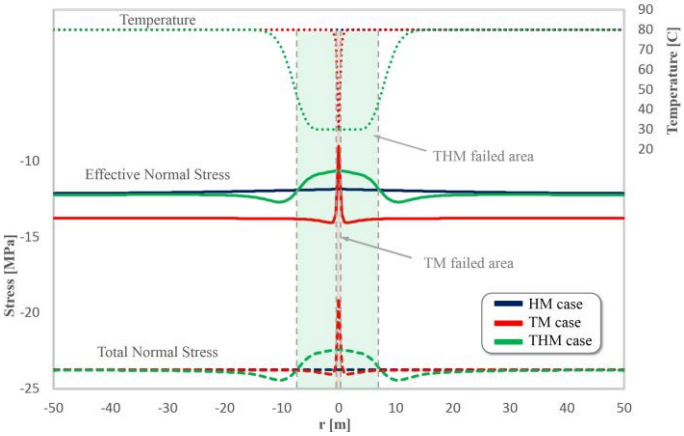

Fig 6. Profiles of total normal stress (dashed line), effective normal stress (solid line), and temperature (dotted line) along the fracture at the end of injection/cooling (i.e. 20 hours) for the three cases (the continuum mechanics convention of compression negative is used for this figure).

5. SENSITIVITY ANALYSIS

It is worthwhile to investigate the effect of in-situ stress conditions and injection parameters on the elastic and failure behavior of a conductive fracture during fluid injection. For this purpose, the three injection/cooling scenarios considered earlier are used as base cases for a sensitivity analysis. Thermal, hydraulic and mechanical properties of the model are same as Table 2, unless stated otherwise.

5.1. Fracture Orientation

In the presence of anisotropic in-situ stress condition, fracture orientation controls the normal and shear stresses acting on the fracture surface. Thus, by changing the fracture orientation, the fracture behavior under different normal stress conditions can be studied. To measure the proximity of a stress-state to failure, we define the Mohr-Coulomb failure index (*MCFI*) as:

$$MCFI = |\sigma_s| - |(\sigma_n + p)\tan\phi| \qquad (4)$$

where σ_n and σ_s are the normal and shear stresses on the fracture surface, respectively, p is the fracture pressure and ϕ is the fracture friction angle. Negative values of the *MCFI* indicate shear stress levels less than required for failure (i.e. the fracture is in the elastically deformable state), whereas positive values of this index correspond to M-C failure.

Profiles of the MCFI values prevailing along the fracture at the end of injection/cooling for the three cases considered earlier are shown in Fig 7 for fracture strikes ranging from zero to 90º with respect to the *x*-axis. The results show that *MCFI* is negative for the HM case, i.e. the fracture is in an elastic, non-slipped state (compliant fracture based on Table 1). For the TM case, the read area in Fig 7 indicates failure occurs in the immediate vicinity of the cooled borehole for fracture orientations between 45º and 75º. As noted earlier, the failed length is limited to the size of a fracture element. For the THM case, failure occurs for fracture orientations between 50º and 70º, with the maximum length of failure of 11.5 occurring at the fracture orientation of 60º. This orientation angle is the angle of the plane with least shear resistance (i.e. 45º+ϕ/2). The M-C failure index as well as fracture failed length at the injection/cooling point (along the dash-dotted line in Fig 7) are shown in Fig 8 for fracture orientations in the range 0º-90º.

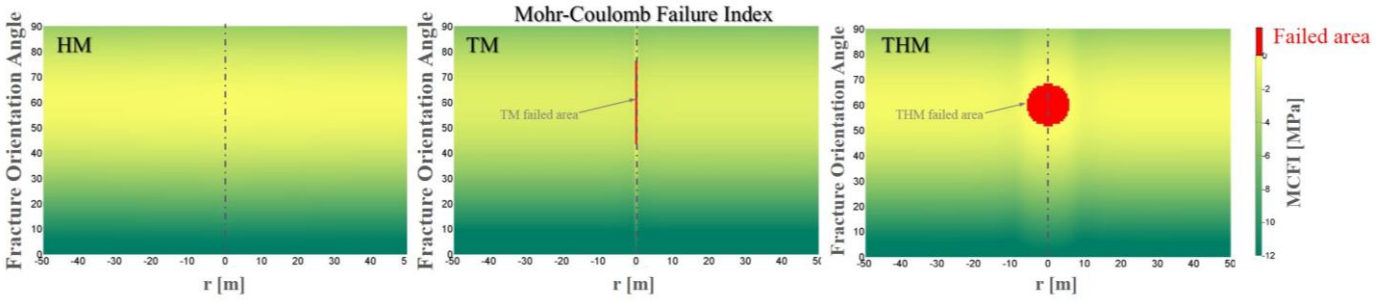

Fig 7. Profiles of the Mohr-Coulomb fracture index for 0-90 degrees range of the fracture orientation under three different injection scenarios, i.e. HM, TM and THM cases after 20 hours. The red color represents positive *MCFI*, indicating failure has occurred.

5.2. Fluid Injection Rate

Fluid injection rate is an interesting parameter to vary because it controls the pressure increment in the fracture. Also, increased flow rate, results in an increase in the (negative) heat flux added to the system through advection. This is evident in Fig 9, where the injection flow rate is increased from 1×10^{-9} $m^3/s/m$ up to 5×10^{-9} $m^3/s/m$. As a consequence the cooled fracture length increases from 5.5 to 24.5 m and failure length defined by positive values of *MCFI*, increases from 2.5 to 21.5 m.

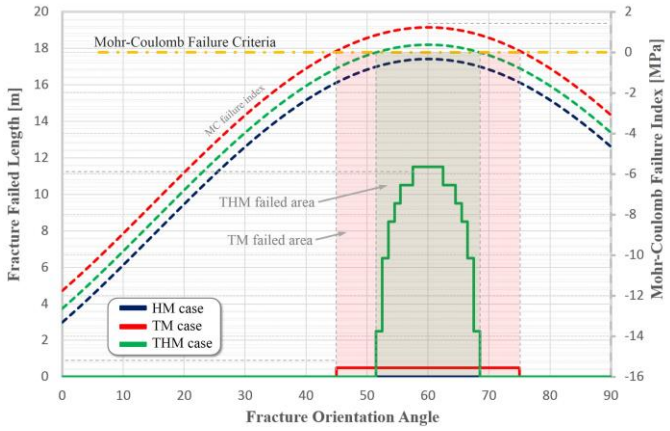

Fig 8. Fracture failed length (solid lines) and Mohr-Coulomb failure index (dashed lines) as a function of fracture orientation. The green and red shaded areas denote the range of failure orientations for the THM and TM cases. The yellow dash-dotted horizontal line at *MCFI* = 0 denotes the M-C failure line.

As the injection rate is decreased below 1×10^{-9} $m^3/s/m$, the THM case converges to the TM case as advective heat transfer becomes insignificant. In this case, an abrupt upturn in normal stress develops around the injection point as the cooling distribution around the injection point approaches radial symmetry of the TM model. This is an artifact which was explained in the previous section. It is useful to mention here that an increase in fracture pressure leads to higher value of *MCFI*. The local minimum of the *MCFI* profile correlates with the margins of the cooled region extending from the borehole.

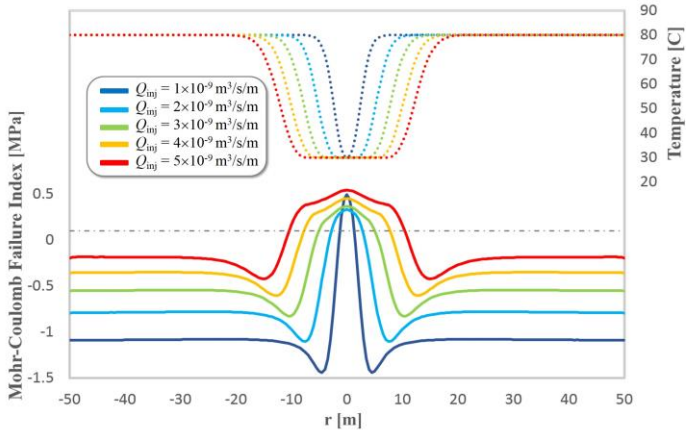

Fig 9. Profiles of Mohr-Coulomb failure index (solid lines) and temperature (dotted lines) along the fracture at the end of injection/cooling (i.e. 20 hours) for different cold fluid injection rates. The gray dash-dotted horizontal line at *MCFI* = 0 denotes the M-C failure line.

5.3. Injection Temperature

It has been shown that injection of fluid that is 50ºC cooler than the rock, into a fracture that is optimally oriented for failure (60º oriented fracture with respect to the *x*-axis in this study) results in the propagation of failure after only several hours (Fig 5). In this section, the effect of different injection temperature on failure behavior is investigated by varying the temperature difference between the fluid and rock from 50ºC to +10ºC. All other parameters are the same as in the base case (i.e. injection rate of 3×10^{-9} $m^3/s/m$). The resulting profiles of temperature and *MCFI* along the fracture after 20 hours injection are shown in Fig 10. Clearly, injecting cooler fluid increases the thermal stress and hence the *MCFI* value. However, positive values of the *MCFI*, which indicate failure conditions have been reached, occur only for $\Delta T \leq$ -25ºC. Even at ΔT = -30ºC, the failure length is significantly less than the length of the cooled zone, in contrast to ΔT = -50ºC where the two lengths are comparable, as noted earlier. Injection of fluid that is warmer than the rock generates a compressive thermal normal stress on the fracture, which leads to fracture pressure rise due to the reduction of the fracture aperture. In this case, the *MCFI* value of the warmed region drops by temperature rise. However, it looks like temperature rise might results in enhancement of the failure potential ahead of the heat front as a consequence of stress conservation (stress redistribution) resulting in the loss of normal stress across the fracture tip region.

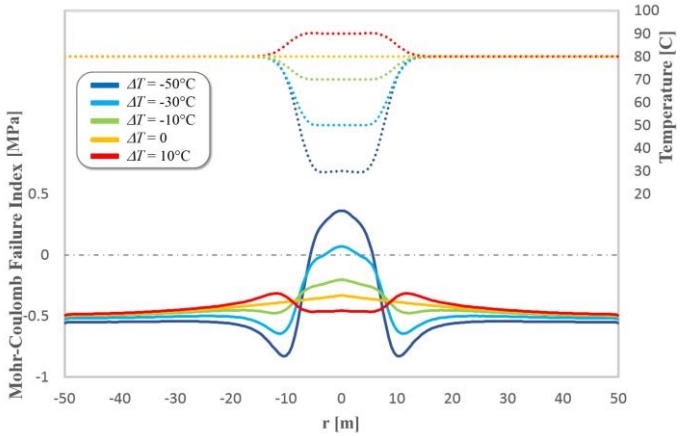

Fig 10. Profiles of Mohr-Coulomb failure index (solid lines) and temperature (dotted lines) along the fracture at the end of injection/cooling (i.e. 20 hours) for different injection temperature. The gray dash-dotted horizontal line at *MCFI* = 0 denotes the M-C failure line.

6. SUMMARY AND CONCLUSION

The elastic deformation and failure behaviour of a conductive fracture undergoing injection of relatively cold fluid was considered in this paper and hydroelastic, thermoelastic and thermo-hydroelastic aspects of the fracture under different injection protocols were studied. A fully coupled, 2-D plane-strain, hybrid numerical model was developed by combining the finite difference method and the displacement discontinuity method. Simulations performed with different stress states acting

on the fracture, and at different injection temperatures and flow rates lead to the following conclusions:

- Fluid injection (Δp) inside a conductive fracture in an impermeable host rock lowers the effective normal stress on the fracture surfaces by fracture pressure increment. Total normal stress on the fracture surface stays constant due to the absence of poroelastic and thermoelastic stresses (HM case).
- Cooling down (ΔT) the rock around the borehole without any fluid injection (TM case) induces an abrupt stress drop adjacent to the heat source. Since there is no flow in the fracture, conduction is the only heat transfer mechanism in the system. Conduction in rock is slow, and the cooling front is radially symmetric, which is a geometry that gives rise to large changes in normal stress, albeit highly localized.
- Cold fluid injection ($\Delta p + \Delta T$) affects the normal stress on the fracture in two different ways: reduction of the total normal stress because of temperature drop (thermoelastic rock matrix shrinkage) and reduction of the effective normal stress due to fluid pressure increase. Combination of these two mechanisms (THM case) can lead to shear slip of the cooled section of the fracture.
- For the cases considered, the thermoelastic effect on failure overwhelms the Δp effect. Beyond the cooled region of the fracture, Δp effect tends to dominate because the pressure front always moves faster than the temperature front, thermoelastic effects manifest themselves as an increase in total stress that tends to inhibit failure.

The results of this work clearly show the importance of both ΔT and Δp effects during injection of relatively cold fluids into a conductive fracture within hot rock. It also reveals that although *T*-propagation lags behind *p*-propagation during injection, its effect on failure could be significant at early times during the injection. Thermomechanical effect may also become dominant over the long term, when enough time has elapsed for the cooling front to propagate significantly from the borehole, as for example, during long term reservoir circulation in an EGS project. In such cases, it is possible that cooling results in permeability enhancement along the propagating cooling path and thus fracture conductivity is enhanced, and large-scale thermoelastic stress redistribution persists over time. This effect is evident in the reduced pressure gradient along the fracture between 10 hours and 20 hours in Fig 3. We should however acknowledge the fact that when a problem becomes this complex (our cases are regular, 2-D, homogenous and isotropic in term of fracture fabric and rock mass parameters), the impact of details of rock mass condition and behavior may evade intuition; hence, modeling results must be carefully scrutinized and verified with monitoring whenever possible to make sure that predictions are realistic.

REFERENCES

1. White, G.P. 1986. *Waterflooding*. TX, United States: Society of Petroleum Engineers.
2. van As, A., and R.G. Jeffrey. 2000. Caving induced by hydraulic fracturing at Northparkes Mines. In *Pacific Rocks*, ed. J. Girard et al., 353-360.
3. Kaiser P.K., B. Valley, M.B. Dusseault, and D. Duff. 2013. Hydraulic fracturing mine back trials - design rationale and project status. In *Effective and Sustainable Hydraulic Fracturing*, ed. A.P. Bunger, J. McLennan, R. Jeffrey, 877-891.
4. Pine R.J., and A.S. Batchelor. 1984. Downward migration of shearing in jointed rock during hydraulic injections. *Int. J. Rock Mech. Min. Sci.* 21(5): 249-263.
5. Coussy, O. 2004. *Poromechanics*. 1st ed. London: John Wiley & Sons.
6. Jalali, M.R. 2013. *Thermo-hydro-mechanical behavior of conductive fractures using a hybrid finite difference – displacement discontinuity method*. Ph.D. thesis, University of Waterloo. Waterloo, ON, Canada.
7. Boussinesq, J. 1868. Mémoire sur l'influence des frottments dans les mouvements réguliers des fluids, *J. Liouville*, 13: 377-424.
8. Witherspoon, P.A., J.S.Y. Wang, K. Iwai, and J.E. Gale. 1980. Validity of cubic law for fluid flow in a deformable rock fracture, *Water Resour. Res.*, 16: 1016-1024.
9. Goodman, R.E. 1976. *Methods of geological engineering in discontinuous rock*. New York: West Publishing Group.
10. Bandis, S.C., A.C. Lumsden, and N.R. Barton. 1983. Fundamentals of rock joint deformation. *Int. J. Rock Mech. Min. Sci.* 20 (6): 249-268.